length of 25 mm, outer diameter of 6.0 mm and inner diameter of 2.3 mm. The acoustic sensor was fabricated from a 20 μm-thick piezoelectric film P(VDF-TrFE) (KF piezo-film, Kureha Corp., Tokyo, Japan), which has a wider frequency bandwidth than that of a lead zirconium titanate piezoelectric ceramic. The PA signal detected by the acoustic sensor was amplified by a low noise field-effect transistor amplifier (SA-220F5, NF Electronic Instruments, Yokohama, Japan) and then recorded by a digital oscilloscope (M9210A, Agilent Technology, Santa Clara, CA) with a sampling rate of 2 GSa/s, and a bit depth of 12 bit.

Low-density polyethylene (LDPE) tubes (T0310, Yamaichi Chemical, Osaka, Japan) with wall thickness of 1.0 mm and inner diameters of 4.0, 5.0, and 6.0 mm filled with optical absorbers were used as blood vessel phantoms. The blood vessel phantoms were immersed in the turbid medium at a depth of 8.0 mm from the turbid medium surface. Mixtures of specific black ink (Black Ink, Pilot, Tokyo, Japan) and intralipid (Intralipid fluid solution 20 %, Fresenius Kabi AB, Germany) were used as optical absorbers and a turbid media. Optical properties of optical absorbers and a turbid media were shown in Table 1. To place the tube phantoms at focal zone of the focused acoustic sensor, we used the degassed water filled in small water tank as an acoustic spacer. The bottom of the small water tank was an 11 μm-thick clear polymer film selected to ensure minimal attenuation of excitation light pulses and PA signals. The bottom of the water tank was on the ambient medium surface. The acoustic sensor was immersed in the degassed water and placed 20 mm away from the tube phantoms. The experiment was performed with excitation pulse energy of 4.0 mJ.

3. RESULTS AND DISCUSSION

3.1 Numerical simulation

A spatial distribution of absorbed optical energies calculated by the light transport simulation is shown in Fig. 2(a). The surface of the turbid medium was z = 12 mm. The top surface of a blood vessel phantom with a diameter of 6 mm and an effective attenuation coefficient of 29.1 cm^{-1} was z = 20 mm. The excitation light irradiated from the top surface of the turbid medium was absorbed by both the turbid medium and the blood vessel phantom.

A simulated PA signal measured by the focused acoustic sensor is shown in Fig. 2(b). PA signals produced from the turbid medium and the tube phantoms were observed at t = 8 μs and 13.3μs, respectively. Figure 3(a) shows the CWT of the PA signal observed at 12 - 16 μs. Two maxima observed in the CWT originate from the positive and the negative peaks of the PA signal waveform, respectively. Figure 3(b) shows dominant frequencies of the PA signal as a function of time. The maximum of the dominant frequency observed at the positive peak of the PA signal was used to quantify the effective attenuation coefficient. Figure 4 shows the parameters as functions of the effective attenuation coefficients of the phantoms. The maximum of dominant frequencies obtained from the PA signals measured by focused acoustic sensor were proportional the effective attenuation coefficient with a correlation coefficient of 0.99, and a slope of 0.035

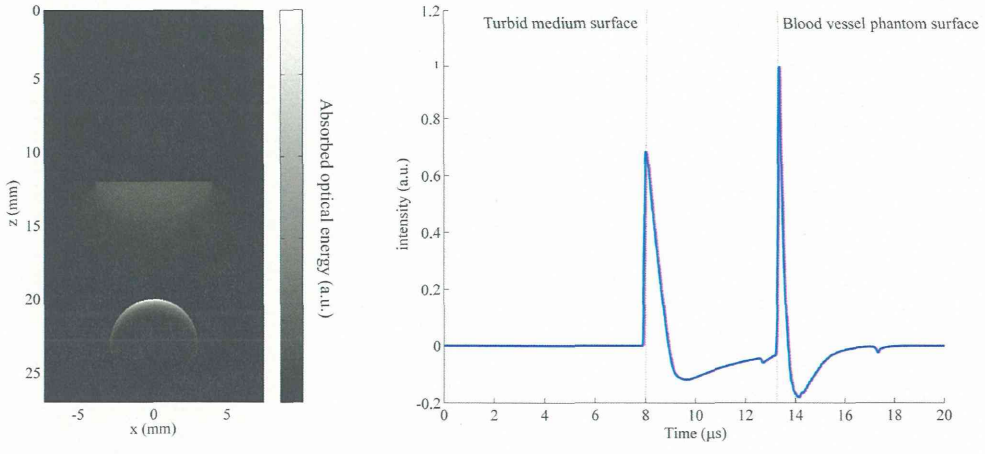

(a) (b)

Fig. 2 (a) Example of simulated spatial distribution of absorbed optical energies and (b) simulated PA signals measured by focused acoustic sensor (b)

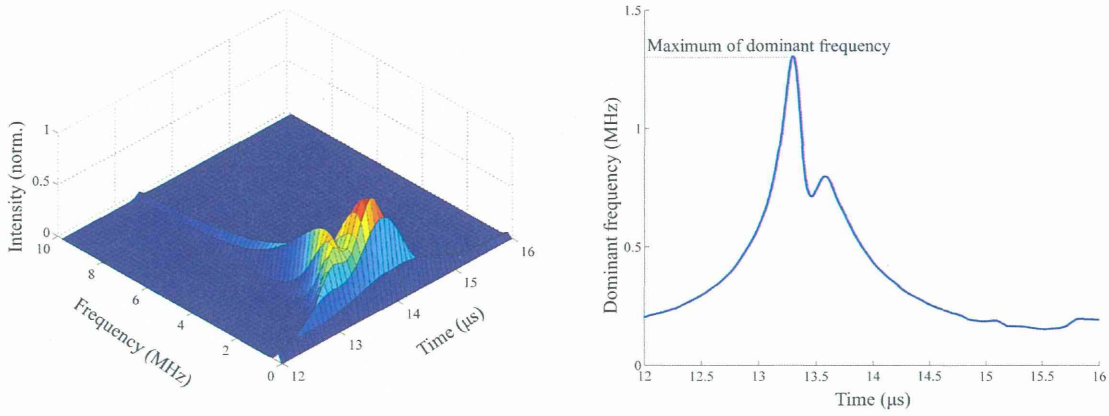

(a) (b)

Fig. 3 (a) CWT of the simulated PA signal (b) dominant frequencies of the PA signal calculated from CWT as a function of time.

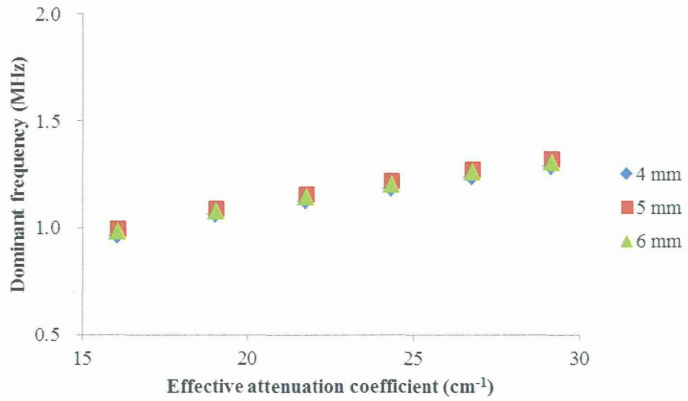

Fig.4 Maximum of the dominant frequencies of simulated PA signals produced from blood vessel phantoms with various diameters as functions of effective attenuation coefficients of optical absorbers.

MHz/cm^{-1}. Additionally, the frequencies were independent of the blood vessel diameters. These results suggest that the maximum dominant frequencies of PA signals produced from blood vessels enable to quantify the effective attenuation coefficients of the blood vessels independently from the blood vessel diameters.

3.2 Experiment using phantoms

PA signals produced from blood vessel phantoms were measured by the focused acoustic sensor. To calculate maximum dominant frequencies, CWTs of the PA signals were calculated. Figure 5 shows the maximum dominant frequencies of the PA signals produced from the phantoms with various diameters as functions of effective attenuation coefficients. Although the frequencies were proportional to the effective attenuation coefficients with correlation coefficient of 0.96, the measured values shown in Fig. 5 were slightly different from the simulated values shown in Fig. 4. This difference is caused by frequency response of the focused acoustic sensor. By convolving the frequency response of the sensor into the simulated PA signal, these results will match. The frequencies shown in Fig. 4 were suffered from deviations of 0.135 MHz. The deviation was caused by slight change of the sensor angle and position. Since slight change of the sensor alignment displaces the sensitive region of the sensor, the sensor measures PA signals produced at different area of the optical absorber. The optical absorber surface within the sensitive area of the sensor strongly affects the frequency of PA signal, because the optical absorber surfaces strongly absorb excitation light. Thus, change of the optical absorber

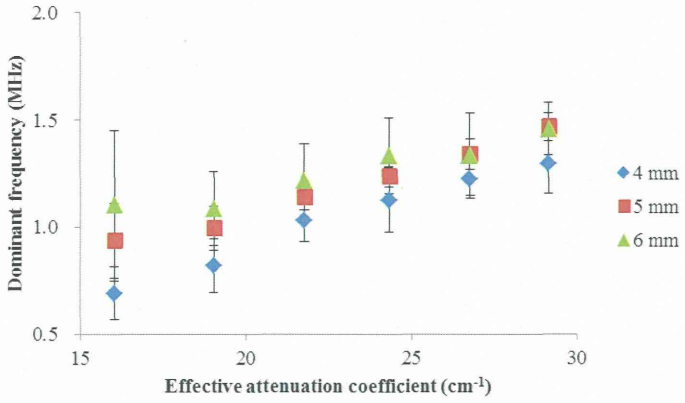

Fig.5 Dominant frequencies of PA signals produced from blood vessel pahntom with various diameters as a function of effective attenuation coefficient (error bar: standard deviation, n=3).

surface within the sensitive region of the sensor due to the slight change of alignment causes the frequency change of PA signals. Since the blood vessel phantom with small diameter have small curvature radius, the PA signal produced from phantoms with small diameters were sensitive to the alignment of the sensitive region of the sensor. Thus, it is necessary to improve robustness to experimental factors such as sensor alignment. In order to reduce the frequency change, the sensitive region of focused acoustic sensor should be sufficiently narrower than the blood vessel diameter. The narrower sensitive region can be obtained by increasing the numerical apertures of focused acoustic sensors. Another approach is extract other parameters from CWTs of PA signals to correct the frequency changes.

4. CONCLUSION

In this paper, we discussed the application of the method of quantifying the effective attenuation coefficients to blood oxygenation monitoring of blood vessels. The method uses the continuous wavelet transform to calculate the time-resolved frequency spectra of photoacoustic (PA) signals. The time resolved frequency spectra of PA signals were affected by geometries of optical absorbers. Numerical simulations of a light transport and ultrasound propagation were performed to calculate temporal waveforms of PA signals produced from blood vessel phantoms with various diameters and optical properties placed in the turbid medium. As results of simulations, by measuring the PA signal from small area, the maximum dominant frequencies of the PA signals calculated by using the CWT were proportional to the effective attenuation coefficient with a correlation coefficient of 0.99, and a slope of 0.035 MHz/cm^{-1}, and the frequencies were independent of the tube diameter. The simulation result suggested that the frequencies of PA signals measured from small area enable to quantify the effective attenuation coefficient of the blood in the blood vessels with various diameters. We also performed experiment using blood vessel phantoms with various diameters. In the experiment, to measure the PA signals from small area, the focused acoustic sensor made of P(VDF-TrFE) was used. As results of the experiments, the maximum dominant frequencies of PA signals calculated from CWTs of the PA signals were proportional to the effective attenuation coefficients of blood vessel phantoms. However, the frequencies were suffered from large deviations of 0.135 MHz. The deviation was caused by slight difference of the sensor alignment because the frequencies of PA signals produced from phantoms with small diameters are sensitive to the sensor alignment. Thus, it is necessary to improve robustness to experimental factors such as sensor alignment. Use of a focused acoustic sensor with higher numerical aperture will enable to reduce the effect of experimental factors such as sensor alignment.

ACKNOWLEDGMENT

This research was partially supported by JSPS KAKENHI Grant Number 25750192 and 25282158, a Health and Labor Science Research Grant for Research on Medical Device Development, and JST Collaborative Research Based on Industrial Demand (In vivo Molecular Imaging : Towards Biophotonics Innovations in Medicine). The authors appreciate the contributions of Mr. Y. Ikeda, and Mr. H. Ishihara to this study. Experiments were supported by the Laboratory Center, National Defense Medical College.

REFERENCES

[1] C. Li, and L. V. Wang, "Photoacoustic tomography and sensing in biomedicine," Phys Med Biol, 54(19), R59-97 (2009).

[2] S. Y. Emelianov, P.-C. Li, and M. O'Donnell, "Photoacoustics for molecular imaging and therapy," Physics today, 62(8), 34 (2009).

[3] A. Taruttis, M. Wildgruber, K. Kosanke *et al.*, "Multispectral optoacoustic tomography of myocardial infarction," Photoacoustics, 1(1), 3-8 (2013).

[4] T. J. Allen, A. Hall, A. P. Dhillon *et al.*, "Spectroscopic photoacoustic imaging of lipid-rich plaques in the human aorta in the 740 to 1400 nm wavelength range," J Biomed Opt, 17(6), 061209-1-061209-10 (2012).

[5] H. F. Zhang, K. Maslov, G. Stoica *et al.*, "Functional photoacoustic microscopy for high-resolution and noninvasive in vivo imaging," Nat Biotechnol, 24(7), 848-51 (2006).

[6] A. d. l. Zerda, Z. Liu, S. Bodapati *et al.*, "Ultrahigh sensitivity carbon nanotube agents for photoacoustic molecular imaging in living mice," Nano letters, 10(6), 2168-2172 (2010).

[7] G. P. Luke, D. Yeager, and S. Y. Emelianov, "Biomedical Applications of Photoacoustic Imaging with Exogenous Contrast Agents," Annals of biomedical engineering, 1-16 (2012).

[8] I. Y. Petrov, Y. Petrov, D. S. Prough *et al.*, "Optoacoustic monitoring of cerebral venous blood oxygenation through extracerebral blood," Biomed Opt Express, 3(1), 125-36 (2012).

[9] H. F. Zhang, K. Maslov, M. Sivaramakrishnan *et al.*, "Imaging of hemoglobin oxygen saturation variations in single vessels in vivo using photoacoustic microscopy," Appl Phys Lett, 90(5), 053901-053901-3 (2007).

[10] B. Cox, J. G. Laufer, S. R. Arridge *et al.*, "Quantitative spectroscopic photoacoustic imaging: a review," J Biomed Opt, 17(6), 061202 (2012).

[11] J. Laufer, B. Cox, E. Zhang *et al.*, "Quantitative determination of chromophore concentrations from 2D photoacoustic images using a nonlinear model-based inversion scheme," Appl Opt, 49(8), 1219-1233 (2010).

[12] J. Laufer, C. Elwell, D. Delpy *et al.*, "In vitro measurements of absolute blood oxygen saturation using pulsed near-infrared photoacoustic spectroscopy: accuracy and resolution," Phys Med Biol, 50, 4409-4428 (2005).

[13] M. Jaeger, M. Hejazi, and M. Frenz, "Diffraction-free acoustic detection for optoacoustic depth profiling of tissue using an optically transparent polyvinylidene fluoride pressure transducer operated in backward and forward mode," J Biomed Opt, 10(2), 024035-024035-7 (2005).

[14] Y. Wang, and R. Wang, "Photoacoustic recovery of an absolute optical absorption coefficient with an exact solution of a wave equation," Phys Med Biol, 53(21), 6167-77 (2008).

[15] Z. Guo, C. Favazza, A. Garcia-Uribe *et al.*, "Quantitative photoacoustic microscopy of optical absorption coefficients from acoustic spectra in the optical diffusive regime," J Biomed Opt, 17(6), 066011 (2012).

[16] T. Hirasawa, M. Fujita, S. Okawa *et al.*, "Improvement in quantifying optical absorption coefficients based on continuous wavelet-transform by correcting distortions in temporal photoacoustic waveforms," Proc. of SPIE, 8581, 85814J (2013).

[17] T. Hirasawa, M. Ishihara, K. Tsujita *et al.*, "Continuous wavelet-transform analysis of photoacoustic signal waveform to determine optical absorption coefficient," Proc. of SPIE, 8223, 822333 (2012).

[18] T. Hirasawa, M. Fujita, S. Okawa *et al.*, "Quantification of effective attenuation coefficients using continuous wavelet transform of photoacoustic signals," Appl Opt, 52(35), 8562-8571 (2013).

[19] P. Addison, J. Watson, and T. Feng, "Low-oscillation complex wavelets," Journal of Sound and Vibration, 254(4), 733-762 (2002).

[20] P. Addison, [The illustrated wavelet transform handbook: introductory theory and applications in science, engineering, medicine] London: Institute of Physics Publishing, (2002).

[21] L. V. Wang, and H.-i. Wu, [Biomedical optics: principles and imaging] John Wiley and Sons, Hoboken, NJ(2007).

[22] S. L. Jacques, and S. A. Prahl, [Absorption Spectra for Biological Tissues (Oregon Medical Laser Center, OR)], (2004).

[23] W. C. Y. Lo, and L. Lilge, "Accelerated 3D Monte Carlo light dosimetry using a graphics processing unit (GPU) cluster," Proc. of SPIE, 737609 (2010).

Quantification of effective attenuation coefficients using continuous wavelet transform of photoacoustic signals

Takeshi Hirasawa,[1,*] Masanori Fujita,[2] Shinpei Okawa,[1] Toshihiro Kushibiki,[1] and Miya Ishihara[1]

[1]Department of Medical Engineering, National Defense Medical College, 3-2, Namiki, Tokorozawa, Saitama 359-8513, Japan

[2]Division of Environmental Medicine, National Defense Medical College Research Institute, 3-2, Namiki, Tokorozawa, Saitama 359-8513, Japan

*Corresponding author: hirasawa@ndmc.ac.jp

Received 11 July 2013; revised 8 November 2013; accepted 13 November 2013; posted 14 November 2013 (Doc. ID 193028); published 6 December 2013

A method for quantifying the effective attenuation coefficients of optical absorbers by using the continuous wavelet transform (CWT) to calculate the time-resolved frequency spectra of photoacoustic signals is proposed. Because the coefficients can be quantified according to the relative intensity of the frequency content of the signals, it is unnecessary to determine the fluences. A computational simulation reveals that the time-resolved frequency spectra exhibit better correlation with the coefficients than do power spectra calculated using a Fourier transformation. The CWT-based method was experimentally verified, and the coefficients were quantified with mean square error of 2.0 cm^{-1}. © 2013 Optical Society of America

OCIS codes: (170.0110) Imaging systems; (170.1460) Blood gas monitoring; (170.2655) Functional monitoring and imaging; (170.5120) Photoacoustic imaging; (170.6935) Tissue characterization.

http://dx.doi.org/10.1364/AO.52.008562

1. Introduction

Photoacoustic imaging (PAI) is a combined ultrasound and optical imaging technique that allows for spatial mapping of optical absorbers in biological tissues. The PAI technique is based on the generation of photoacoustic (PA) pressure waves, which generate ultrasound waves when the optical absorber material absorbs excitation light—generally, pulsed laser beams that satisfy thermal and stress confinement requirements. These PA pressure waves propagate through biological tissues and can be measured as PA signals by acoustic sensors. By calculating the distances between the acoustic sensors and the optical absorbers using the speed of sound in the biological tissues and the time delay from the laser excitation time, a spatial mapping of the optical absorbers can be obtained.

Because oxy-hemoglobin and deoxy-hemoglobin are dominant optical absorbers in biological tissues at wavelengths of 700–900 nm, both produce strong PA signals over this wavelength range, which serves as an optical window that allows light to penetrate up to several centimeters into biological tissues [1]. Oxy-hemoglobin and deoxy-hemoglobin are know to have different optical absorption spectra [2–4], so PA signals measured at multiple excitation wavelengths can be used to distinguish between the two [5]; accordingly, measurement of PA signals can be used to determine the blood oxygen saturation, or the ratio of oxy-hemoglobin to total hemoglobin.

1559-128X/13/358562-10$15.00/0

Measuring the blood oxygen saturation in this manner has the advantages of higher spatial resolution and noninvasiveness compared to conventional methods such as pulse oximetry or gas analysis [6]. To calculate the blood oxygen saturation from PA signals, the optical absorption coefficient or effective attenuation coefficient of blood should be quantified at each excitation wavelength [3]. Considerable attention has been paid to developing methods for quantifying the values of these coefficients in optical absorbers [3,7–9]. The effective attenuation coefficient μ_{eff} can be expressed as follows:

$$\mu_{\text{eff}} = \{3\mu_a(\mu_a + \mu_s')\}^{\frac{1}{2}}, \quad (1)$$

where μ_s' is the reduced optical scattering coefficient, and μ_a is the optical absorption coefficient. Because the optical energy densities (fluences) affect PA signals, it is necessary to remove their effects in order to quantify the optical absorption coefficients or effective attenuation coefficients of optical absorbers [7].

The amplitude of a PA signal can be calculated as the product of the optical absorption coefficient, the fluence on the surface of the absorber, and a proportional factor called the Grüneisen parameter, which expresses the efficiency of conversion from heat to ultrasound energy. Because the Grüneisen parameter is assumed to be constant in most cases [3], the optical absorption coefficient can usually be calculated by dividing the PA signal amplitude by the product of the optical absorber surface fluence and the Grüneisen parameter. Owing to the strong optical scattering in biological tissues, however, the fluence on the surface of the optical absorber is usually unknown. One method for quantifying the optical absorption coefficient is to solve the radiative transfer equation and the PA wave equation [10]. However, the methods used to solve these equations typically involve a computationally intensive iterative algorithm, making it difficult to quantify the coefficient in real time.

To overcome these barriers, temporal PA signal waveforms that depend on the depth profiles of the absorbed optical energies [8,11,12] can be used to quantify the effective attenuation coefficients of optical absorbers. Because optical energy attenuates exponentially along the light transfer axis of an optical absorber, the temporal waveform of a PA signal detected along the light transport axis will have an exponentially attenuated form. One major advantage of the temporal waveform method is that the effective attenuation coefficients can be quantified on the basis of the relative temporal attenuation profiles of the PA signals, making it unnecessary to determine the fluences on the optical absorber surface. By using limited detection modes, the effective attenuation coefficients of an optical absorber can be quantified by fitting the temporal waveforms of PA signals to the exponential attenuation functions [10]. There are two limited detection modes: near-field detection, in which the PA signals can be considered to be plane waves [11,12], and forward-mode detection, in which the sample is irradiated by an excitation light source located on the far side of the acoustic sensor [3]. Neither of these, however, is considered appropriate for measuring deep regions of thick biological tissue.

PA signal frequency spectra have also been used to derive the effective attenuation coefficients of optical absorbers [9,13]. Frequency spectra, which are generally calculated using the Fourier transform (FT), efficiently extract the features of PA signal temporal waveforms. Because PA signals are unsteady pulsed waves, they have time-varying frequency content; however, as the FT has no time resolution, only the time-averaged frequency spectra are calculated. This blurs the temporal change of the frequency contents of the PA signals. Thus, frequency analysis of PA signals should employ time-resolved methods.

In this paper, we propose the use of the continuous wavelet transform (CWT) to calculate the time-resolved frequency spectra from the temporal waveforms of PA signals [14,15]. The CWT, which can produce time-resolved frequency spectra, is widely used to analyze unsteady signals with time-variable frequency content. Indeed, previous studies have already used the wavelet transform to reduce PA signal noise; for instance, Viator and others used the discrete wavelet transform to reduce white noise from PA signals [16–18], and Li *et al.* and others used CWT to calculate the band-pass filtered PA signal characteristics over various frequency ranges in order to determine which frequency band offers the maximum signal-to-noise ratio [19–21]. However, we could not find any studies in which the CWT was used for frequency analysis rather than noise reduction.

In this study, we analyzed the relationship between the time-resolved frequency spectra of PA signals and the effective attenuation coefficients of optical absorbers, as these correlations strongly affect the accuracy of quantification. We then calculated the coefficients of optical absorbers using the time-resolved frequency spectra of PA signals measured by our original PA measurement system [22]. Finally, these calculated values were compared with the values determined by two methods; one uses the frequency spectra of PA signals calculated using FT, and another uses the temporal waveform of the PA signals.

2. Theoretical Background

A. Detection of PA Signal

PA pressure waves consist of ultrasound energy packets produced by an optical absorber that has absorbed short laser pulses. Assuming that the laser pulsewidths are much shorter than the thermal diffusion time in the optical absorber and that the acoustic inhomogeneity and viscosity of the medium are negligible, the wave equation of the PA pressure $p(\mathbf{r}, t)$ (Nm^{-2}) can be given as [1,23]

$$c^2\nabla^2 p(\mathbf{r},t) - \frac{\partial^2 p(\mathbf{r},t)}{\partial t^2} = \frac{\beta c^2}{C_p}\frac{\partial H(\mathbf{r},t)}{\partial t}, \quad (2)$$

where c(m/s) is the speed of sound in the medium, β(K^{-1}) is the isobaric volume expansion coefficient, C_p(J/g K) is the specific heat, and $H(\mathbf{r},t)$ (Jm^{-3}) is the heat energy generated by optical absorption. The solution to Eq. (1) in the time domain can generally be expressed as [1]

$$p(\mathbf{r}',t) = \frac{\beta}{4\pi C_p}\iiint \frac{\mathrm{d}^3\mathbf{r}}{|\mathbf{r}-\mathbf{r}'|}\frac{\partial}{\partial t'}H(\mathbf{r},t')\Big|_{t'=t-|\mathbf{r}-\mathbf{r}'|/c}, \quad (3)$$

where $\mathbf{r}'$ is the observation point. The heat energy $H(\mathbf{r},t)$ can be expressed as the product of the spatial mapping of the absorbed optical energy $A(\mathbf{r})$ and the temporal waveform of the laser pulse $\eta(t)$, allowing Eq. (2) to be rewritten in spherical coordinates as a convolution of the temporal waveform of the laser pulse $\eta(t)$ and a PA waveform excited by a Dirac delta pulse [1,8,24]:

$$p(\mathbf{r}',t) = \frac{\beta}{4\pi C_p}\left(\frac{1}{t}\iint_{|\mathbf{r}-\mathbf{r}'|=ct} A(\mathbf{r}-\mathbf{r}')\mathrm{d}S\right) * \eta'(t), \quad (4)$$

where $\eta'(t)$ is the first time derivative of the temporal profile of the excitation laser pulse. The PA signal $s(\mathbf{r},t)$ detected by an acoustic sensor with an impulse response of $m(t)$ can be expressed as

$$s(\mathbf{r}',t) = \frac{\beta}{4\pi C_p}\left(\frac{1}{t}\iint_{|\mathbf{r}-\mathbf{r}'|=ct} A(\mathbf{r}-\mathbf{r}')\mathrm{d}S\right) * \eta'(t) * m(t). \quad (5)$$

3. Materials and Methods

A. Experimental Setup

We used a reflection mode PA measurement system in which the excitation light irradiation and PA signal detection occur on the same side of the sample, as this detection mode is more appropriate for measuring deep regions of thick biological tissue [22]. A block diagram of this measurement system is shown in Fig. 1. A tunable Ti:sapphire laser (LT-2211, Lotis Tii, Minsk, Belarus) pumped by the second harmonic of a Q-switched Nd:YAG laser (LS-2134, Lotis Tii, Minsk, Belarus) was used to produce excitation light pulses with a width of 20 ns and a repetition frequency of 15 Hz at a wavelength of 720 nm. The excitation pulses were then coupled into a multimode optical fiber with a core diameter of 0.4 mm (M40L02, Thorlabs, Newton, New Jersey).

The optical fiber was arranged coaxially relative to a specially designed ring-shaped acoustic sensor (coaxial PA probe) [22] with inner and outer detection surface diameters of 1.4 and 3.0 mm, respectively. Using a coaxial PA probe made it possible to detect the PA signal along the light transport axis. The

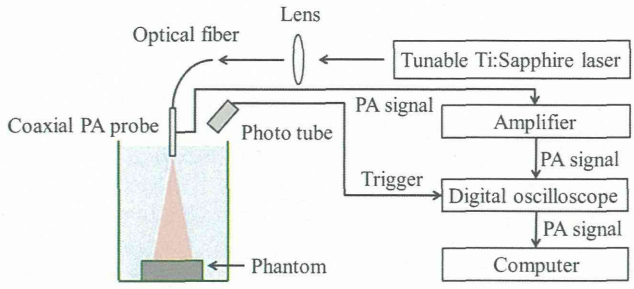

Fig. 1. Experimental setup for reflection mode measurement of PA signals.

acoustic sensor was fabricated from a 50-μm-thick piezoelectric film P(VDF-TrFE) (KF piezo-film, Kureha Corp., Tokyo, Japan), which has a wider frequency bandwidth than that of a lead zirconium titanate piezoelectric ceramic [22]. The acoustic sensor was already calibrated within the frequency range of 1–20 MHz by a secondary calibration method [25] using a precalibrated hydrophone (HPM05/3, Precision Acoustics, Dochester, UK). The frequency of maximum sensitivity was 1.7 MHz, and the 6 dB frequency band was 1.2–14.4 MHz. Using an acoustic sensor with such a wide frequency bandwidth enabled us to analyze the spectra of the PA signals over a wide frequency range. The PA signals detected by the acoustic sensor were amplified by a low-noise field-effect transistor amplifier (SA-220F5, NF Electronic Instruments, Yokohama, Japan) and then recorded by a digital oscilloscope (DSO8104A, Agilent Technology, Santa Clara, California) with a sampling rate of 2 GSa/s.

B. Computational Simulation

To calculate the relationship between the frequency spectra of the PA signals and the effective attenuation coefficients of optical absorbers, we used Eq. (4) as the basis for an analytical simulation of the generation of PA pressure waves and the detection of PA signals. In the model, PA pressure waves were generated by irradiating planar optical absorbers with excitation light pulses (pulsewidth = 20 ns) via an optical fiber. The resulting PA signals were detected by a ring-shaped acoustic sensor with inner and outer detection surface diameters of 1.4 and 3.0 mm, respectively. The acoustic sensor and optical fiber were coaxially combined and placed at a distance of 45 mm from the optical absorber.

Because optical scattering in the optical absorber was neglected for the purposes of this simulation, the effective attenuation coefficients, μ_{eff}, were proportional to the optical absorption coefficients μ_a. Thus, the amount of optical energy $A(r,\theta,\varphi)$ absorbed by an optical absorber with an absorption coefficient of μ_a could be formulated using spherical coordinates as

$$A(r,\theta,\phi) = \frac{r\sin\theta}{r_0\sin\theta_0}F(r_0\cos\theta\cos\phi, r_0\cos\theta\sin\phi) \times \exp\left(-\int_0^r \mu_a(r',\theta,\phi)\mathrm{d}r'\right), \quad (6)$$

$$\mu_a(r,\theta,\phi) = \mu_a \quad \text{where } r\cos\theta < z_0, \tag{7}$$

where F is the fluence of the excitation light pulses measured by a beam profiler (SP620, Ophir, Israel), which is placed on the surface 17.5 mm from the output end of the optical fiber. The optical absorption coefficients μ_a were varied over a range of 10–40 cm^{-1}, which corresponds to the effective attenuation coefficients of blood over a wavelength range of 700–900 nm with a hematocrit concentration of 40%–50% and an oxygen saturation of 0%–100% [3].

Because the time increment of this simulation was 3 ns, the Nyquist frequency was 166 MHz, which is sufficiently higher than the frequencies of the PA signals. The size and shape of the detection surface were taken into account by performing a surface integration process in which the detection surface was discretized into small elements and the PA signals detected by each element were calculated using Eq. (4). Finally, the individual signals were numerically integrated in order to calculate the total PA signal detected by the sensor surface.

The impulse response function of the acoustic sensor was measured, and then incorporated into the simulated PA signals. The impulse response function $m(t)$ was obtained by measuring a PA signal produced at a spatial point [8,26]. The PA signal was produced by irradiating an excitation pulse focused by a convex lens with focal length of 200 mm onto carbon suspension with an optical absorption coefficient of 2000 cm^{-1}. Because the excitation pulse was absorbed within a volume smaller than the ultrasound wavelength, the optical absorption distribution $A(\mathbf{r}-\mathbf{r}')$ in Eq. (4) can be approximated by Dirac's delta function $\delta(\mathbf{r}-\mathbf{r}')$. Thus, the PA signal can be expressed as follows using Eq. (5):

$$s_\delta(\mathbf{r}',t) = \frac{\beta}{4\pi C_p}\frac{1}{|\mathbf{r}-\mathbf{r}'|}\eta'\left(t-\frac{|\mathbf{r}-\mathbf{r}'|}{c}\right) * m(t). \tag{8}$$

Thus, by substituting the following equation into Eq. (5), the impulse response function of the acoustic sensor was incorporated into the simulation:

$$m(t) * \eta'(t) = \frac{4\pi C_p}{\beta}|\mathbf{r}-\mathbf{r}'|s_\delta\left(\mathbf{r}',t+\frac{|\mathbf{r}-\mathbf{r}'|}{c}\right). \tag{9}$$

C. Experiment Using Phantoms

To verify the relationship between the frequency spectra of the PA signals and the effective attenuation coefficients of optical absorbers, we measured the PA signals produced by phantoms having various optical absorption coefficients. Because of its resistance to photobleaching, a specific black ink (Black Ink, Pilot, Tokyo, Japan) was used as an optical absorber. The ink was diluted with water down to six different concentrations. The diluted black inks were then placed in a cylindrical container with a diameter of 35 mm and a thickness of 9 mm, and the top surface of the container was sealed with an 11-μm-thick clear polymer film selected to ensure minimal attenuation of excitation light pulses and PA signals. The coaxial PA probe was placed perpendicular to the top surface of the phantom at a distance of 45 mm, and then both the phantom and the probe were immersed in degassed water. The experiment was performed with excitation pulse energies of 300, 600, and 1200 μJ.

The optical attenuation coefficients of the diluted inks quantified from the PA signals were compared with the optical attenuation coefficients measured using a spectrophotometer (U-3300, Hitachi High-technologies, Tokyo, Japan)

D. Frequency Analysis of PA Signals

The CWT is a spectral analysis method that can produce time-resolved frequency spectra of PA signals. This method differs from the FT, which produces a frequency spectrum without time resolution. The CWT modulus of a signal $T(a,b)$ is defined as the convolution of the temporal signal $p(t)$ and the dilated and temporally translated version of the wavelet function $\Psi(t)$ [14,17,27–30]:

$$T(a,b) = a^{-\frac{1}{2}}\int_{-\infty}^{\infty} p(t)\Psi^*\left(\frac{t-b}{a}\right)dt, \tag{10}$$

where $\Psi^*(t)$ is the complex conjugate of $\Psi(t)$, a is the dilation parameter, and b is the location parameter. Here, the complex Morlet wavelet, which is defined as a complex sinusoid with a Gaussian envelope [15,28,30], is used:

$$\Psi(t) = \pi^{-\frac{1}{4}}(e^{-i\omega_0 t} - e^{-\omega_0^2 t})e^{-\frac{t^2}{2}}, \tag{11}$$

where ω_0 is the central frequency of the wavelet, which determines the number of sinusoidal waves within the Gaussian envelope. The dilation parameter a can be transformed into the frequency f using the equation $f = \omega_0/a$, where the time t replaces the location parameter b. Thus, the CWT produces time-resolved frequency spectra $T(f,t) = T(\omega_0/a,b)$ with a power given by $|T(f,t)|^2 = \mathrm{Re}[T(f,t)]^2 + \mathrm{Im}[T(f,t)]^2$.

The time-resolved spectra were compared with the power spectra of the PA signal, which were calculated using the FT. The FT was applied to the PA signals cropped with a rectangular window with a time width of 4 μs. This time width was wider than the recording length. A frequency resolution of 10 kHz was achieved by padding the PA signal with zeros.

4. Results

A. Computational Simulation

PA signals produced by optical absorbers with effective attenuation coefficients of between 10 and 40 cm^{-1} were calculated; Fig. 2 shows the temporal

waveforms of the signals produced by the absorbers with coefficients of 17 and that of 30 cm^{-1}. Although the leading edges of the PA signals shown in the figure have nearly identical slopes, their trailing edges differ; this suggests that only the trailing edges of PA signals depend on the effective attenuation coefficients of the optical absorbers. The time-resolved frequency spectrum of the PA signal produced by the optical absorber with an effective attenuation coefficient of 17 cm^{-1} is displayed in Fig. 3(a), which shows the peaks of the PA signal temporal waveforms observed at time $t = 0$. The local maxima originating from both positive and negative parts of the temporal waveform were observed at t_1 and t_2, respectively.

The profiles of the time-resolved frequency spectrum at times t_1 and t_2 are displayed in Fig. 3(b). The dominant frequencies were determined by calculating the frequencies satisfying $d|T(f,t)|^2/df = 0$ and are shown in Fig. 4 as functions of time. The dominant frequencies in the figure all have maximum values at time $t = -0.015$ μs, which coincides nearly perfectly with the peak time of the temporal waveform; it is therefore apparent that the maximum values of the dominant frequencies depend on both the leading and trailing edges of the PA signals. Because the slopes of the trailing edges of the signals depend on the effective attenuation coefficients of the optical absorbers, we can use the maximum values of the dominant frequencies to quantify these coefficients.

The maximum values of the dominant frequencies and the peak frequencies of the power spectra are shown in Fig. 5 as functions of the effective attenuation coefficients of the optical absorbers. The peak frequencies of the power spectra are shown in Fig. 5. Owing to the variation in the acoustic sensor sensitivity at frequencies of less than 1 MHz, the peak frequency of the power spectra varied nonlinearly with the effective attenuation coefficients of the

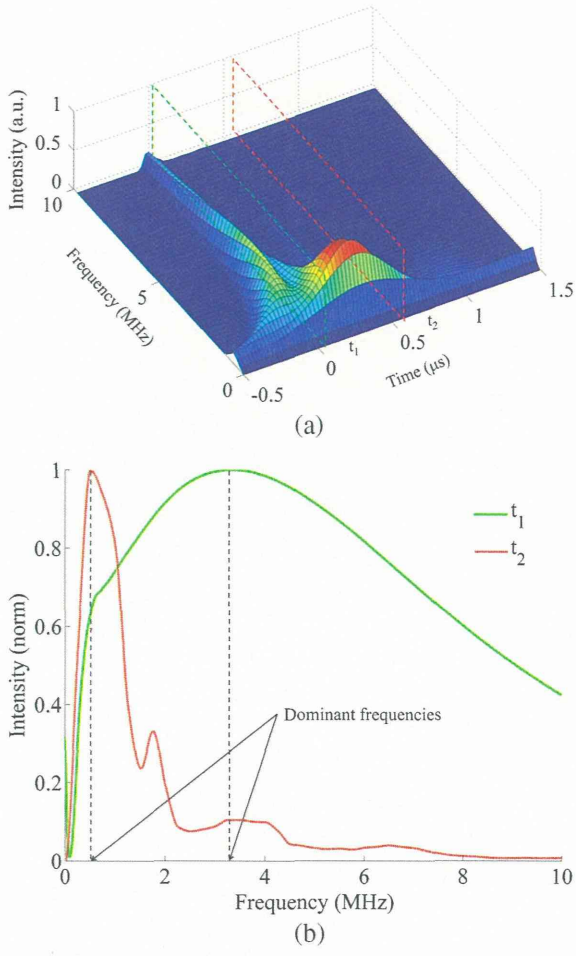

Fig. 3. Analysis of calculated PA signals produced by an optical absorber with an effective attenuation coefficient of 17 cm^{-1}. (a) Time-resolved frequency spectra of PA signal calculated using CWT. The maxima originating from the positive and negative parts of the PA signal were observed at times t_1 and t_2, respectively. (b) Profiles of time-resolved frequency spectra with respect to times t_1 and t_2

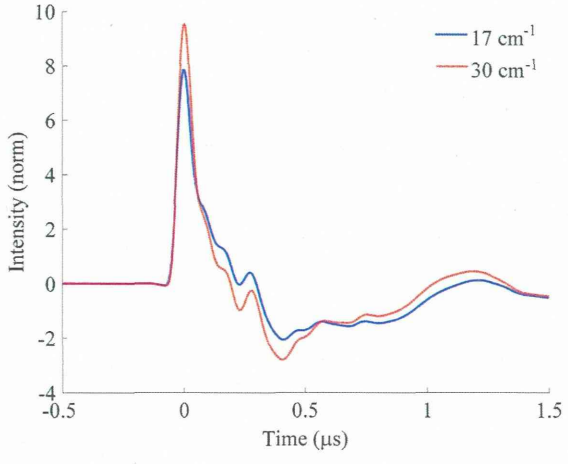

Fig. 2. Temporal waveforms calculated for PA signals produced by optical absorbers with effective attenuation coefficients of 17 cm^{-1} (blue) and 30 cm^{-1} (red), respectively. The amplitudes of the PA signals are normalized.

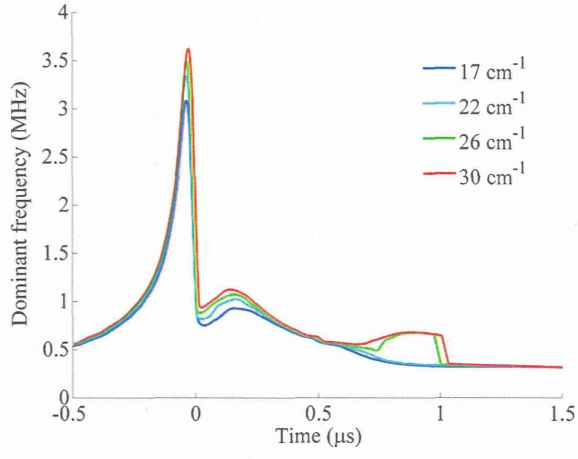

Fig. 4. Dominant frequency of the PA signal produced from optical absorbers with various effective attenuation coefficient as a function of time.

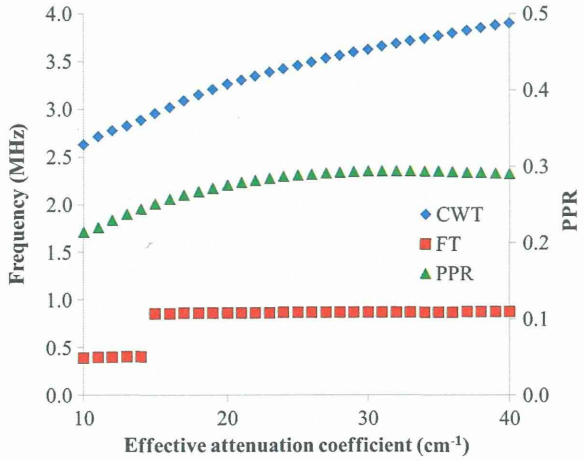

Fig. 5. Relationship between the maximum values of dominant frequencies of calculated PA signals and the effective attenuation coefficients of optical absorbers (blue, diamond). The peak frequencies of power spectra calculated by using FT (red, square) and PPR calculated from temporal waveform (green, triangle) are also plotted.

optical absorbers. The maximum values of the dominant frequencies, in contrast, monotonically increased as the coefficient increased.

We also calculated the peak-to-peak ratio (PPR) of the temporal waveform, which is defined as the ratio of the positive peak and negative peaks. Wang and Wang proposed to use this parameter to determine the optical absorption coefficient [8]. The peaks of the dominant frequencies and the PPRs are shown in Fig. 4 as functions of the effective attenuation coefficients of the optical absorbers. Both parameters increased as the coefficient increased. However, the PPR became constant for an effective attenuation coefficient larger than 30 cm^{-1}.

B. Experiment

PA signals produced by phantoms consisting of diluted black inks with six concentrations were measured using a coaxial PA probe. The effective attenuation coefficients of the diluted inks measured using a spectrophotometer were 13, 17, 22, 26, 30, and 35 cm^{-1}.

The time-resolved frequency spectrum of the PA signal produced by the optical absorber with an effective attenuation coefficient of 13 cm^{-1} is displayed in Fig. 6(a), which shows the peaks of the PA signal temporal waveforms observed at time $t = 0$. The profiles of the time-resolved frequency spectrum at times t_1 and t_2 are displayed in Fig. 6(b). The dominant frequencies are shown in Fig. 7 as functions of time. The dominant frequencies calculated from the CWT, the peak frequencies calculated from the FT of the PA signals, and the PPR are displayed in Fig. 8. Both the dominant frequency and the PPRs of the measured PA signals coincided with those of the simulated PA signals. The peak frequencies of the PA signals calculated using the FT exhibited no correlation with the effective attenuation coefficients of the optical absorbers.

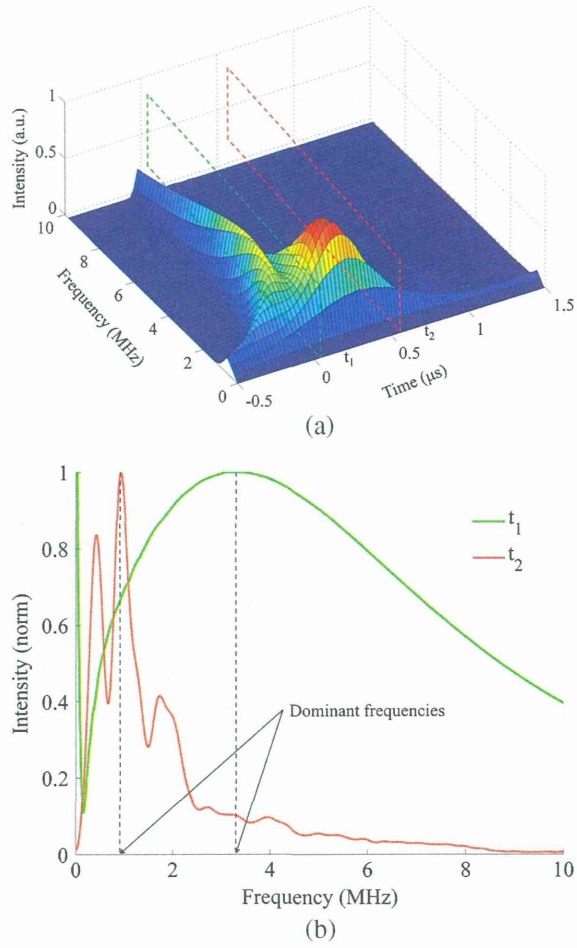

Fig. 6. Analysis of experimentally measured PA signals produced by an optical absorber with an effective attenuation coefficient of 17 cm^{-1}. (a) Time-resolved frequency spectra of PA signal calculated using CWT. The maxima originating from the positive and negative parts of the PA signal were observed at times t_1 and t_2, respectively. (b) Profiles of time-resolved frequency spectra with respect to times t_1 and t_2.

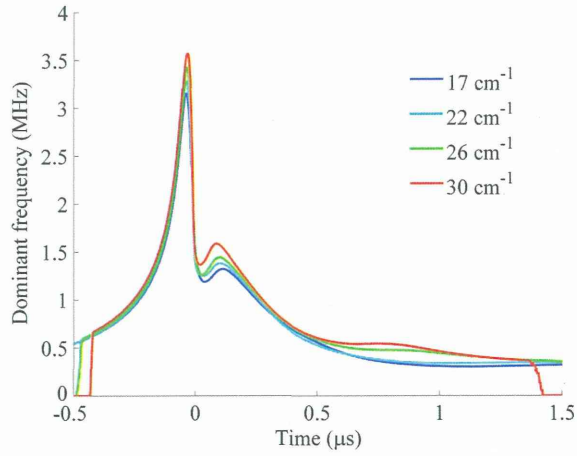

Fig. 7. Dominant frequency of the PA signal produced from optical absorbers with various optical absorption coefficients as a function of time.